IJE TRANSACTIONS A: Basics Vol. 33, No. 7, (July 2020) 1403-1412

International Journal of Engineering

Journal Homepage: www.ije.ir

Numerical Analysis of Grease Film Characteristics in Tapered Roller Bearing Subject to Shaft Deflection

Z. H. Wu, Y. Q. Xu*, K. A. Liu, Z. Y. Chen

School of Mechatronical Engineering, Northwestern Polytechnical University, Xi'an 710072, China

P A P E R I N F O

Paper history:
Received 24 May 2020
Received in revised form 07 June 2020
Accepted 12 June 2020

Keywords:
Film Characteristics
Grease Lubrication
Shaft Deflection
Tapered Roller Bearing

A B S T R A C T

The shaft deflection is one of critical factors that deteriorate the grease lubrication state inside the tapered roller bearings (TRBs). So, in this paper, on the premise of the TRB subjected to the combined loads and the shaft is deflected, the grease lubrication model at the TRB contacts was constructed, in which the interaction loads, linear and angular displacements of the bearing parts were involved. Then the grease film characteristics were numerically analyzed from the perspective of the whole bearing to clarify the negative effects of the shaft deflection on grease film characterizes. The results show that the effect of the shaft deflection on the load distribution in the absence of the radial load is greater than that in the presence of the radial load. The angular misalignment of the roller is mainly affected by the deflection. The deflection results in an irregular film shape and pressure profile at the TRB contacts, and induces a significant pressure spike and necking feature at the roller-end.

***doi**: 10.5829/ije.2020.33.07a.28*

NOMENCLATURE

E_r, E_b	Elastic modulus of roller and rings	$\dot{\gamma}$	Shear rate
F_a	Constant preload force	δ_a	Constant preload displacement
F_x, F_y, F_z	External forces	δ_f	Contact deformation at flange
M_y, M_z	External moments	δ_i	Contact deformations at cone
P_h	Hertzian contact pressure	δ_i	Contact deformations at cup
b_h	Half Hertzian contact width	δ^*	Geometric constant
c_v	Sum of the principal curvatures	ς_r, ς_{bi}	Radii of roller and cone
g, g_r, g_b	Geometric clearances	ρ	Grease density
h	Grease film thickness	τ	Grease shear stress
h_0	Rigid body displacement	τ_y	Grease yield viscosity
h_p	Thickness of plug flow layer	υ_b	Poisson's ratio of rings
l_e	Roller effective length	υ_r	Poisson's ratio of roller
m	Roller number	φ	Grease plastic viscosity
n	Grease flow index	ω_i	Cone rotation speed
p	Grease film pressure	ω_s, ω_p	Roller rotation and revolution speeds
s	Roller slice number	**Subscript**	
u_{ex}, u_{ex}	Entrainment speeds	i	Reference coordinate system o_i-$x_iy_iz_i$
u_x, u_y, u_z	Cone linear displacements	b	Cone fixed coordinate system o_b-$x_by_bz_b$
v_x, v_y, v_z	Roller linear displacements	r	Roller fixed coordinate system o_r-$x_ry_rz_r$
Greek Symbols		c	Contact coordinate systems o_c-$x_cy_cz_c$
Ω	Analysis area	**Superscript**	
α_h	Roller half cone angle	i	cone
β, θ, ϕ	Roller rotation, tilt and skew angles	o	cup
γ, λ	Deflection angle	f	flange

*Corresponding Author Institutional Email: *xuyngqng@nwpu.edu.cn* (Y. Q. Xu)

Please cite this article as: Z. H. Wu, Y. Q. Xu, K. A. Liu, Z. Y. Chen, Numerical Analysis of Grease Film Characteristics in Tapered Roller Bearing Subject to Shaft Deflection, International Journal of Engineering (IJE), IJE TRANSACTIONS A: Basics Vol. 33, No. 7, (July 2020) 1403-1412

1. INTRODUCTION

Tapered roller bearings, as a separate bearing, can withstand combined radial and thrust loads, and widely exist in high-speed trains, automobiles, rolling mills and other machines. In most of these machines, the grease is commonly adopted as a lubricant to reduce bearing friction, for it can simplify designs of sealing devices and lubricating systems. [1] However, due to the installation error, the mass on the shaft, and the load from the gear system, etc., the bearing shaft would be more or less deflected. [2, 3] The deflected shaft in turn occasions bearing parts (rollers and rings) in a misaligned state, and results in disordered spatial position and uneven load distribution. Ultimately, it inevitably deteriorates the grease lubrication inside the bearing [4, 5]. In addition, coupled with the non-Newtonian properties of the grease, the lubrication problem of the TRB subjected to shaft deflection becomes more complicated. Therefore, the behavior of the grease film inside the TRB when the shaft is deflected should be clarified, which would expand lubrication theory and benefit lubrication design for the TRBs.

The literatures focused on negative effects of the shaft deflection on bearing performances mainly emphasized on the displacements, load-carrying, and fatigue life, etc., [2, 6-12] while on impacts of the misaligned shaft on oil or grease lubrication of the TRB are relatively deficient. [13-17] Harris [2] presented a representative load-deformation relationship to evaluate effects of the shaft misalignment on fatigue life reduction of cylindrical roller bearings. Similar to Harris's method, Zantopulos [6] studied the misaligned shaft's effects on bearing capacity and fatigue life of the TRBs. However, centrifugal force and gyroscopic moment of the rollers were neglected. Andréason [7] presented a vector method to investigate load distribution inside the misaligned TRB. Similarly, the inertial loads of the rollers were not addressed. Liu [8] further extended Andréason's works and considered the inertial loads. De Mul et al. [9] presented an analytical model for equilibrium and associated load distribution in TRBs. Although the model allowed five degrees of freedom for loads and displaces, the roller profile crowning is not considered. Based on De Mul's theory, Tong et al. [10-12] analyzed the stiffness, fatigue life and running torque with the effects of the combined loads and shaft deflection. The above-mentioned works can provide a reference for the grease lubrication analysis of the misaligned TRB. Kushwaha et al. [13] provided a solution for the finite line concentrated contact of a cylindrical roller-to-race under aligned and misaligned states. The oil-lubricated contact is subject to an elastohydrodynamic regime of lubrication under isothermal conditions. Panovko [14] presented a numerical method to study the effect of the roller misalignment on the film pressure and thickness of the oil lubricant in the contact region of the crowned roller pair. Liu et al. [15, 16] separately investigated effects of the roller tilt and skew on the oil-lubricated roller/race interface in the cylindrical roller bearing. The cylindrical roller is a constant cross-section structure, which is quite different from the tapered roller. Wu et al. [17] analyzed grease lubrication at misaligned tapered roller pair, and found that in the case of relatively large radius ratio of contact rollers, the tilt's effect on the film characterizes is more serious than the skew's.

All the above studies on lubrication use a simplified contact model of a pair of rollers, not from the perspective of the whole bearing. Therefore, in this paper, the responses of loads and displacements of the TRB parts with deflected shaft were analyzed first. Then, with regard of the TRB responses, the structure features of the bearing, and the grease-rich lubrication, the grease film characterizes inside the misaligned TRB were numerically studied in the whole bearing perspective.

2. THEORETICAL FORMULATION

2. 1. Load-carrying of TRB The TRB is a kind of roller bearings with strong structural nonlinearity. Assuming the cup is macroscopically stationary, as depicted in Figure 1, the reference system o_i-$x_iy_iz_i$ is arranged at the mass center of the cone, the cone fixed system o_b-$x_by_bz_b$ coincides with the o_i-$x_iy_iz_i$ system under unloaded condition. The external force and moment the TRB carried are $\mathbf{F}_e=[F_x,F_y,F_z]^T$ and $\mathbf{M}_e=[0,M_y,M_z]^T$. The shaft deflection is caused by the moment $\mathbf{M}_e$, and means that the geometric axis o_b-x_b of the bearing unparallel to the rotation axis o_i-x_i. In o_i-$x_iy_iz_i$, linear displacements of the cone and the roller are $\mathbf{w}_i=[u_x,u_y,u_z]^T$ and $\mathbf{v}_i=[v_x,v_y,v_z]^T$. Attitude angles of the cone and roller in their respective fixed systems are $\boldsymbol{\varepsilon}_b=[0,\gamma,\lambda]^T$ and $\boldsymbol{\kappa}_r=[\beta,\theta,\phi]^T$. The γ and λ are shaft deflection angles; the β, θ and ϕ are rotation, tilt and skew angles of the tapered roller, respectively.

For the roller/race assembly, as shown in Figure 1(b, c), the interaction is dealt with the slicing method [1]. For each slice, the Palmgren's load-deformation relationship is adopted [18], that is

$$q_{i,o} = 0.7117\delta_{i,o}^{\frac{10}{9}}\left(\frac{1-\upsilon_r^2}{E_r}+\frac{1-\upsilon_b^2}{E_b}\right)^{-1}\left(\frac{l_e}{s}\right)^{\frac{8}{9}} \quad (1)$$

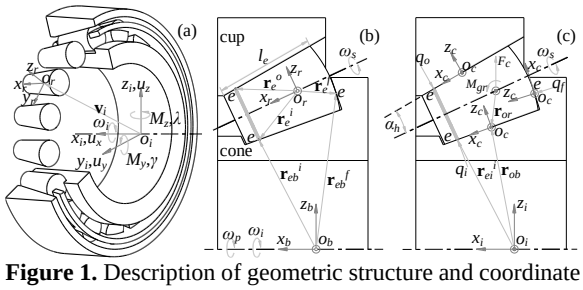

Figure 1. Description of geometric structure and coordinate system of the TRB

If profile crowning of the roller is considered, the crown drop should be subtracted from the roller radius, the crown drop σ along the roller length is [19]:

$$\sigma(l)=\begin{cases}\frac{k_0}{l_1+l_2}\left[l_1+l_2\left(0.8864+ln\frac{1}{\alpha}+ln\frac{l_2-l_1}{l_1}\right)\right], & l=l_1\\ k_0\left\{1+\frac{l}{l_1+l_2}\left[1.7727+2\,ln\frac{1}{\alpha}+ln\frac{(l_2-l)(l-l_1)}{l^2}\right]\right\}, & l_1<l<l_2\\ \frac{k_0}{l_1+l_2}\left[l_2+l_1\left(0.8864+ln\frac{1}{\alpha}+ln\frac{l_2-l_1}{l_2}\right)\right], & l=l_2\end{cases} \quad (2)$$

where l_1 and l_2 are generatrix lengths from the small end and the large end to the taper vertex of the roller, l_e=l_2-l_1; l stands for generatrix length at the contact point e; k_0 and α are coefficients and explicated in [19].

For the flange/roller-end assembly, it is a typical elliptical contact, the interaction force is [18]:

$$q_f=\frac{\pi c_v}{3}\left(\frac{1-v_r^2}{E_r}+\frac{1-v_b^2}{E_b}\right)^{-1}\left(\frac{2\delta_f}{\delta^* c_v}\right)^{\frac{3}{2}} \quad (3)$$

Since the roller's skew has little effect on grease film [18], in order to simplify the model, the skew and the friction at the bearing contacts were not considered. In the contact systems o_c-$x_cy_cz_c$, the interaction forces at the TRB contacts can be rewritten as vector forms.

$$\mathbf{Q}_i=\left[0,0,q_i\right]^T,\mathbf{Q}_o=\left[0,0,-q_o\right]^T,\mathbf{Q}_f=\left[0,0,q_f\right]^T \quad (4)$$

For equilibriums of tapered rollers, centrifugal force F_c and gyroscopic moment M_{gr} are included. Thus:

$$\sum_{k=1}^{s}\boldsymbol{T}_{ci}^{i}\mathbf{Q}_i+\sum_{k=1}^{s}\boldsymbol{T}_{ci}^{o}\mathbf{Q}_o+\boldsymbol{T}_{ci}^{f}\mathbf{Q}_f+\boldsymbol{T}_{ri}[0,0,F_c]^T=\mathbf{0} \quad (5)$$

$$\sum_{k=1}^{s}\boldsymbol{r}_e^{i}\times\boldsymbol{T}_{cr}^{i}\mathbf{Q}_i+\sum_{k=1}^{s}\boldsymbol{r}_e^{o}\times\boldsymbol{T}_{cr}^{o}\mathbf{Q}_o+\boldsymbol{r}_e^{f}\times\boldsymbol{T}_{cr}^{f}\mathbf{Q}_f+\left[0,M_{gr},0\right]^T=\mathbf{0} \quad (6)$$

where $\mathbf{T}_{ci}^{\,i,o,f}$ are conversion matrices from contact coordinate systems o_c-$x_cy_cz_c$ at the cone, cup, and flange to the o_i-$x_iy_iz_i$ system; $\mathbf{T}_{cr}^{\,i,o,f}$ are conversion matrices from the systems o_c-$x_cy_cz_c$ to the roller fixed system o_r-$x_ry_rz_r$; $\mathbf{T}_{ri}$ is conversion matrix from o_r-$x_ry_rz_r$ to o_i-$x_iy_iz_i$; $\mathbf{r}_e^{\,i,o,f}$ are locations of contact points e in o_r-$x_ry_rz_r$.

Simultaneously, the equilibrium for the cone is:

$$\sum_{j=1}^{m}\left[\sum_{k=1}^{s}\boldsymbol{T}_{ci}^{i}\mathbf{Q}_i+\boldsymbol{T}_{ci}^{f}\mathbf{Q}_f\right]+\boldsymbol{F}_e=\mathbf{0} \quad (7)$$

$$\sum_{j=1}^{m}\left[\sum_{k=1}^{s}\boldsymbol{r}_{eb}^{i}\times\boldsymbol{T}_{cb}^{i}\mathbf{Q}_i+\boldsymbol{r}_{eb}^{f}\times\boldsymbol{T}_{cb}^{f}\mathbf{Q}_f\right]+\boldsymbol{M}_e=\mathbf{0} \quad (8)$$

where $\mathbf{T}_{ci}^{\,i,f}$ are conversion matrices from the systems o_c-$x_cy_cz_c$ at the cone and flange to the o_i-$x_iy_iz_i$ system; $\mathbf{T}_{cb}^{\,i,f}$ are conversion matrices from the systems o_c-$x_cy_cz_c$ to o_b-$x_by_bz_b$; $\mathbf{r}_{eb}^{\,i,f}$ are locations of contact points e in o_b-$x_by_bz_b$.

The equilibrium Equations (5)-(8) contain 4m+5 displacement quantities and were solved with the Newton-Raphson method. The process can refer to [11]. The obtained TRB responses will be included in the lubrication model below.

2. 2. Governing Equations of Grease Lubrication

It is assumed that the grease adheres uniformly to the working surfaces of the TRB. The rheological behavior of the grease can be described with the Herschel-Bulkey (H-B) constitutive model, that is

$$\tau=\tau_y+\varphi\dot{\gamma}^n \quad (9)$$

As presented in Figure 2, the lubrication analysis at the roller/race interface was performed in a rectangular area Ω in the o-xy plane, and the o-xyz system is fixed in the reference system and coincides with the o_c-$x_cy_cz_c$ system under unloaded state. Based on the H-B model, Navier-Stokes equation and continuity condition of fluid, the steady state of the grease Reynolds equation is

$$\frac{\partial(\rho G_R)}{\partial x}+\frac{\partial(\rho V_R)}{\partial y}=\frac{\partial(\rho u_{ex}h)}{\partial x}+\frac{\partial(\rho u_{ey}h)}{\partial y} \quad (10)$$

where

$$G_R=\frac{n}{2n+1}\left(\frac{1}{\phi}\frac{\partial p}{\partial x}\right)^{\frac{1}{n}}\left(\frac{h-h_p}{2}\right)^{1+\frac{1}{n}}\left(h+\frac{nh_p}{2n+1}\right) \quad (11)$$

$$V_R=\frac{n}{2n+1}\left(\frac{1}{\phi}\frac{\partial p}{\partial y}\right)^{\frac{1}{n}}\left(\frac{h-h_p}{2}\right)^{1+\frac{1}{n}}\left(h+\frac{nh_p}{2n+1}\right) \quad (12)$$

where h_p indicates thickness of plug flow layer, which is generated due to yield behavior of the grease. Referring to the boundary condition between sheared and non-sheared flow layers, that is, τ =τ_y, h_p is deduced as:

$$h_p=\frac{2\tau_y}{\sqrt{\left(\partial p/\partial x\right)^2+\left(\partial p/\partial y\right)^2}} \quad (13)$$

The film shape h at the roller/race interface is

$$h(x,y)=h_0+g(x,y)+\frac{1}{\pi E^*}\iint_{\Omega}\frac{p(\xi,\zeta)d\xi d\zeta}{(x-\xi)^2+(y-\zeta)^2} \quad (14)$$

Since the cup is stationary, the clearance $g(x,y)$ at the roller/cup interface is easier to be determined. For the roller/cone interface, both the roller and the cone are disordered. To describe the clearance, the point in the o-xyz system is first marked on the roller/cone before the bearing is disordered. After the marked point moved with the roller/cone, its changed position in o-xyz can be known.

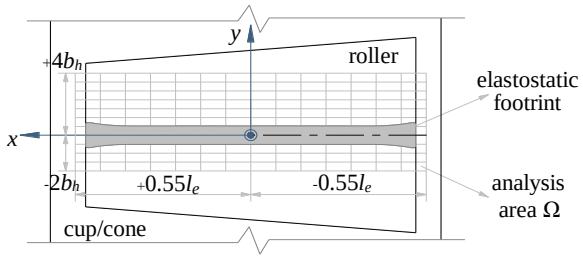

Figure 2. lubrication analysis area at the race contact

Similarly, the marked points $[x_r,y_r,z_r]^T$ and $[x_b,y_b,z_b]^T$ on the roller/cone can be deduced from the changed point $[x,y]^T$ in the regular analysis area Ω in the *o-xy* plane. That are:

$$[x_r, y_r, z_r]^T = \boldsymbol{T}'_{cr0}\{\boldsymbol{T}_{ir}(\boldsymbol{T}'_{ic}[x, y, 0]^T - \boldsymbol{v}_i) - \boldsymbol{r}_{or}\} \quad (15)$$

$$\left[x_b, y_b, z_b\right]^T = \mathbf{T}'_{cb0}\left\{\mathbf{T}_{ib}\left(\mathbf{T}'_{ic}\left[x, y, 0\right]^T - \mathbf{w}_i\right) - \mathbf{r}_{ob}\right\} \quad (16)$$

where $\mathbf{r}_{or,ob}$ are locations of the origin *o* in the roller and cone fixed systems, respectively; $\mathbf{T}_{cr0,cb0}$ denote conversion matrices for the ordered bearing.

The marked points $[x_r,y_r]$ and $[x_b,y_b]$ are the points in the *o-xy* plane before the bearing is disordered. Then, initial surface clearances of the roller and the cone to the *o-xy* plane are:

$$g_r(x_r, y_r)|_{(x,y)} = k_e\varsigma_e(x_r, y_r) - \sqrt{k_e^2\varsigma_r(x_r, y_r)^2 - x_r^2} \quad (17)$$

$$g_b(x_b, y_b)|_{(x,y)} = \sqrt{k_e^2\varsigma_{bi}(x_b, y_b)^2 - x_b^2} + k_e\varsigma_{bi}(x_b, y_b) \quad (18)$$

where k_e is equivalent coefficient of roller radius ς_r and inner-race radius ς_{bi} projected into the *o-yz* plane,

$$k_e = \frac{1 + 2\sin^2\alpha_h + \sin^4\alpha_h \sec 2\alpha_h}{\cos\alpha_h + \sin\alpha_h \tan 2\alpha_h} \quad (19)$$

After the bearing is loaded, the changed clearances $g_r(x,y)$ and $g_b(x,y)$ are:

$$[x, y, g_r(x, y)]^T = \boldsymbol{T}_{ic}\{\boldsymbol{T}'_{ir}(\boldsymbol{T}_{cr0}[x_r, y_r, g_r(x_r, y_r)]^T + \boldsymbol{r}_{cr}) + \boldsymbol{v}_i\} \quad (20)$$

$$[x, y, g_b(x, y)]^T = \boldsymbol{T}_{ic}\{\boldsymbol{T}'_{ib}(\boldsymbol{T}_{cb0}[x_b, y_b, g_b(x_b, y_b)]^T + \boldsymbol{r}_{cb}) + \boldsymbol{u}_i\} \quad (21)$$

Then the clearance $g(x,y)$ is $g_b(x,y)$-$g_r(x,y)$, and linear and angular displacements of bearing parts are contained.

Surface speeds on the roller and races are [20]:

$$\boldsymbol{u}_r^{i,o} = \boldsymbol{T}_{ir}\boldsymbol{T}_{ic}^{i,o'}\{[\omega_s, 0,0]^T \times \boldsymbol{r}_e^{i,o}\} \quad (22)$$

$$\boldsymbol{u}_b^i = \boldsymbol{T}_{ic}^i\left\{\left(\boldsymbol{T}'_{ib}[\omega_i, 0,0]^T - \left[\omega_p, 0,0\right]^T\right) \times \boldsymbol{r}_{ei}^i\right\} \quad (23)$$

$$\boldsymbol{u}_b^o = \boldsymbol{T}_{ic}^o\left\{\left[\omega_p, 0,0\right]^T \times \boldsymbol{r}_{eb}^o\right\} \quad (24)$$

Then entrainment speeds u_{ex} and u_{ey} with which the grease is swept into the race contact are

$$u_{ex} = \left.\frac{\mathbf{u}_r + \mathbf{u}_b}{2}\right|_x, u_{ey} = \left.\frac{\mathbf{u}_r + \mathbf{u}_b}{2}\right|_y \quad (25)$$

The viscosity- and density-pressure relationships are detailed in [17]. The grease film pressure over the area Ω should meet the normal contact force. That is:

$$\sum_{k=1}^{s} q_{i,o} = \iint_{\Omega} p(x, y)\mathrm{d}x\mathrm{d}y \quad (26)$$

Due to the spherical structure of the roller-end, the flange/roller-end assembly is still an elliptical contact under bearing state or shaft deflection. In fact, the bearing and deflection primarily affect the value of the interaction force q_f. Therefore, the lubrication at this assembly was not addressed in the article.

As shown in Figure 2, a rectangular computational domain for the analysis of film behavior at the race contact is defined, inlet and outlet limits are located at $4b_h$ and $-2b_h$, respectively, and side limits are located in $-0.55l_e \le x \le 0.55l_e$. Boundary conditions of the film pressure p are $p \ge 0$ and $p(x,4b_h)=p(\pm 0.55l_e,y)=0$. The Reynolds equation was numerically simulated with the multi-grid method [21], in which the film pressure was iterated by the Gauss-Seidel method and the surface elastic deformation was solved with the DC-FFT method [22]. A total of 3 grid layers are arranged, where the number of nodes on the densest grid layer is 361(*o-y* axis)×1025(*o-x* axis). The iterative errors of the pressure and load are respectively required less than 1×10^{-4} and 1×10^{-5}.

3. COMPUTATIONAL RESULTS

The parameters of the TRB and the grease are detailed in Table 1. It is assumed that the rollers are evenly distributed in the bearing and symmetrically distributed about the o_i-z_i axis. In view of this, only radial load F_z in the o_i-z_i axis is considered, and F_y=0. The shaft deflection is an angular displacement caused by applied moment, so the load-carrying capacity and lubrication state of the TRB can be analyzed under different deflection angles. Generally, as a separable bearing, the TRB needs to be preloaded by a constant axial force F_a or displacement δ_a to ensure its normal service.

3. 1. Constant Force Preload Under the premise of constant force preloaded and no radial load applied, as depicted in Figure 3(a-c), the impact of the deflected shaft on the load-carrying of the TRB is manifest. The load on part of tapered rollers is increased several times compared to the bearing in the aligned state (γ=0), while the other part is in a 'relaxed' state. The distributions of the contact force at the races and flange are the same, and have same tendency to change with the shaft deflection. The contact force at the outer-race is slightly larger than that at the inner-race. This is due to the centrifugal force and gyroscopic moment of the roller. In Figure 3(d), the rollers are all in a negative tilted state ($\theta\approx$-0.005mrad) when the shaft is aligned. The farther away from the o_i-y_i axis, the more severe the roller is tilted when the shaft is

TABLE 1. Parameters of the TRB and the grease

Bearing parameters	**Value**
Bearing inner diameter [mm]	130.00
Bearing outer diameter [mm]	230.00
Bearing width [mm]	70.00
Number of rollers	17
Roller length [mm]	42.06
Roller average diameter [mm]	21.37
Roller half-cone angle [deg]	5.00
Radius of roller spherical end [mm]	153.95
Outer-race contact angle [deg]	15.00
Inner-race contact angle [deg]	5.00
Flange contact angle [deg]	83.00
Elastic modulus of roller and rings [GPa]	2.06
Poisson's ratio of roller and rings	0.30
Bearing speed [krpm]	3.50
Grease parameters	**Value**
Density [kg/m^3]	872
Yield stress [Pa]	153.14
Plastic viscosity [Pa·s^n]	1.7830
Flow index	0.6943

deflected. In Figure 3(e), the deflection shortens effective contact length l_c at the roller/cup interface. In [11, 12], the TRB's inner diameter is 30mm and deflection can reach 5mrad. In this analysis, that are 130mm and ±1mrad. Compared with the deflection's effect in [11, 12], it can be speculated that if the TRB with a large inner diameter, the allowable shaft deflection should be smaller.

The misalignment of the TRB induced by the shaft deflection or external loads would disturb the film forming at the bearing contacts. Figure 4 illustrates the film characteristics at the most-loaded tapered roller, i.e., No. 1 and 9 rollers (the rollers are numbered clockwise, and the No. 1 roller is at 0). The white arrow represents the grease flow direction, and the film thickness and pressure are dimensionless, i.e. $H= h\varsigma_a/b_h^2$, $P=p/P_h$, $\varsigma_a=$ 11.97mm, b_h=0.21mm, P_h=0.97GPa, the same below. It can be seen that the grease film deviated from the normal state (the case of γ=0). The misalignment of the shaft causes a serious tilt of the roller. As the contact area is reduced, it leads to a decrease in film thickness and an increase in film pressure. The thin-film or high-pressure area at tilted rollers exhibits an approximately triangular shape. Due to larger equivalent radius and higher swept speed (Equation (24)), the film at the roller/cup interface is thicker [20]. Note that typical necking feature appears at the outlet region, even if the tapered rollers is in a severely tilted state.

Figure 5 presents the grease film thickness when the shaft deflected at -1mrad. Under combined effect of the loads and displacements, the grease film around the race shows a regular change. Similarly, the film exhibits the necking feature at the outlet region. In particular, the load carried by No. 1~2 rollers are small, for degraded action area and roller's contact length, a severe tilt still induces a thinner film. Figure 6 reveals the film characterizes along the o_c-x_c axis. A notable necking feature and pressure spike occurs at the contact end, and it resembles the stress edge effect to some extent. [1] The pressure peak p_m fluctuates greatly and it is higher at the cone. Although the film at the outer-race is thicker, as shown in Figure 6, it is not much different in thickness at the inner-race. The pressure p_m may cause stress concentration in the subsurface of the roller or races, thereby reducing the fatigue life of the bearing.

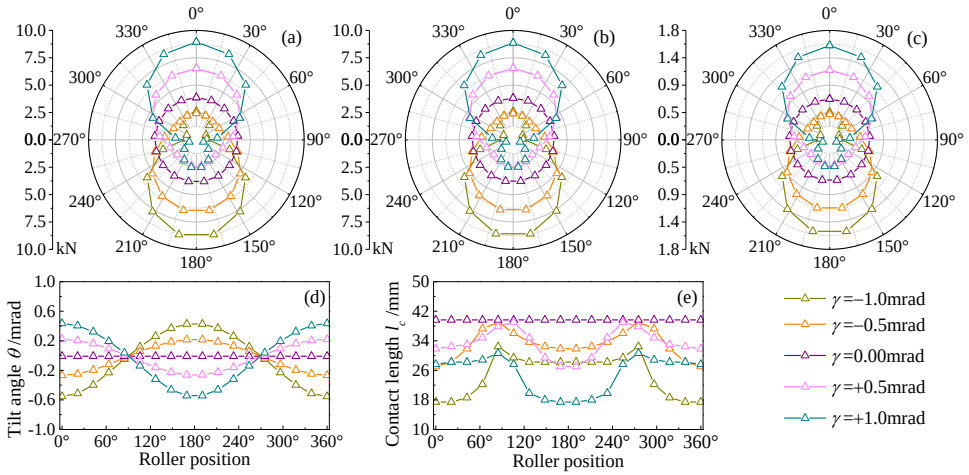

Figure 3. Bearing condition of TRB under constant force preload. F_a=17kN, F_z=0. Normal force (a) at the outer-race, (b) at the inner-race, (c) at the flange. (d) tilt angle, (e) contact length at the outer-race

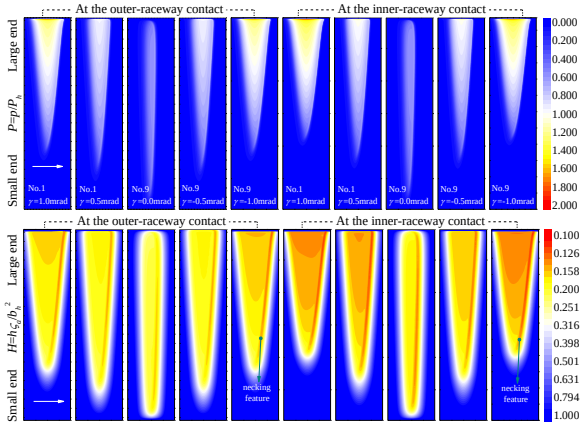

Figure 4. Grease film characterizes of the most loaded roller

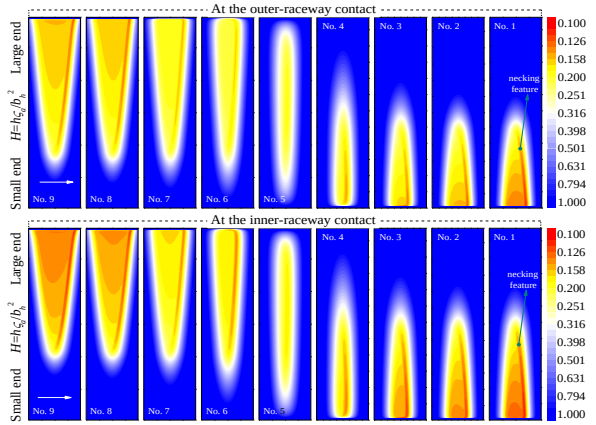

Figure 5. Film thickness at the race contacts when γ=-1mrad

In Figures 4 and 5, for one of the tilted tapered rollers, either the large or small end is in contact with the cone and the cup at the same time, instead of two ends being in contact with the cone and cup, respectively. Compared with Figure 3(e), the contact length of the roller at hydrodynamic contact is longer than that at dry contact; this confirms the bearing function of grease film.

When the TRB carries the radial load F_z, in Figure 7(a), it is substantially in a half-turn bearing state [10]. The force distribution is less affected by the misaligned shaft, which quite differs from the case with no radial load in Figure 3(a). Variations of the force distribution at the races and the flange with the shaft deflection are the same (the variations are not drawn here). In Figure 7(b), the tilted state of the tapered rollers coincides with the result in Figure 3(d), the rollers are still in a severe tilted state due to the shaft deflection. The amplitudes of the tilt angle are substantially similar, whether the radial load F_z is applied or not. However, in Figure 7(c), the effect on the effective contact length at the roller/race interface is remarkable. The contact length when the shaft is aligned is generally longer than that when the shaft is deflected. Although the radial load F_z reduces the contact length of the roller in the relaxed half-circle (γ=0), it has a slight effect on the roller tilt and the rollers are tilted in -0.015~-0.022mrad.

Under the loading state of F_a=28kN and F_z=-43kN, Figure 8(a) reveals the film conditions at the roller/cup interface of the highest loaded No. 9 roller. Due to the misalignment of the roller or shaft, the film thickness and pressure at the roller squeezed section are respectively reduced and increased. This is consistent with the results in [13]. With the shaft deflected from +1mrad to -1mrad, the tilt angle of the roller θ is -0.54, -0.27, -0.02, 0.22 and 0.44mrad. The film pressure peak p_m transfers from the small end to the large end and is 2.32, 1.80, 0.93, 1.53 and 1.88GPa. That is, the pressure p_m is positively correlated with the tilt angle θ. When γ=0, the tilt angle θ is -0.02mrad and is relatively small, the shape of the thin-film area is mainly related to the non-equal cross-section structure of the bearing. Figure 9(a~e) presents the film characteristics along the o_c-x_c axis. Although the tilt angle and the carried load of the roller are huge in the case of negative tilt (θ<0), the overall film pressure is smaller

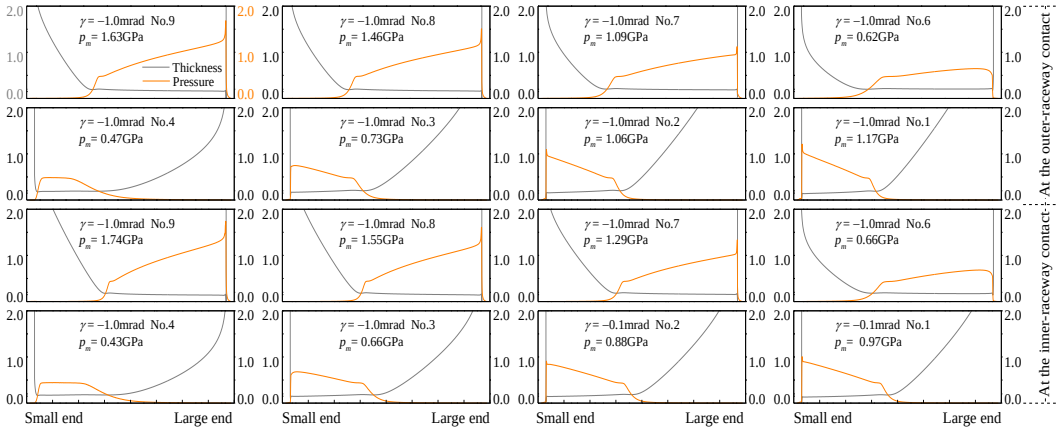

Figure 6. Grease film shape and pressure profile at y=0 when γ=-1mrad

than that in the positive tilted state (θ>0). This is due to the large radius section coming into contact when the tapered roller is in negative tilt. In fact, it indicates that the crown drop at the small radius section of the roller should be larger than the large radius section.

In addition, when the shaft deflection is -1mrad, film behaviors of the rollers at different positions are revealed in Figure 8(b). The film exhibits a regular change, and the necking feature is still remarkable at the outlet region. Even though some rollers subjected to a lower load, such as No. 1~3 rollers, the large tilt angle θ still induces a thinner grease film. The elastostatic footprint of light-loaded rollers is relatively narrow. In Figure 9(e~l), the film pressure spike and the necking feature appear at the roller-ends, especially for the rollers far away from the o_i-y_i axis. The pressure peak p_m is in the range of 0.63~1.88GPa. As with the results in Figure 6, the edge pressure is increased several folds. This is consistent with the results in [17]. It indicates that the efficacy of the roller profile crowning (Equation (2)) is weakened. Therefore, the misalignment of the shaft or roller should be properly considered when designing the profile of the roller. In the above analysis, it seems that the TRB's angular displacement has more pronounced effect on grease film than the linear displacement. In fact, any displacements will essentially affect the interaction at the contacts, thus affecting the film-forming performance. [13, 14]

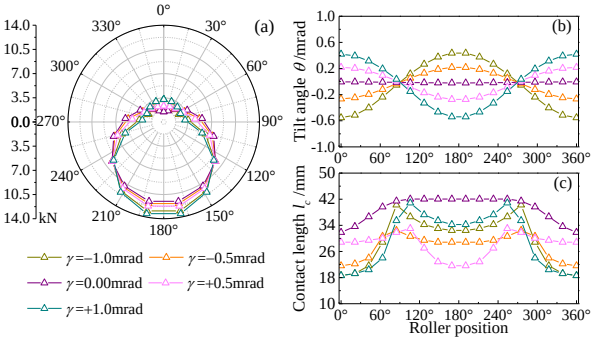

Figure 7. Bearing condition of the TRB under constant force preload. F_a=28kN, F_z=-43kN. (a) contact force at the outer-race. (b) tilt angle. (c) contact length at the outer-race

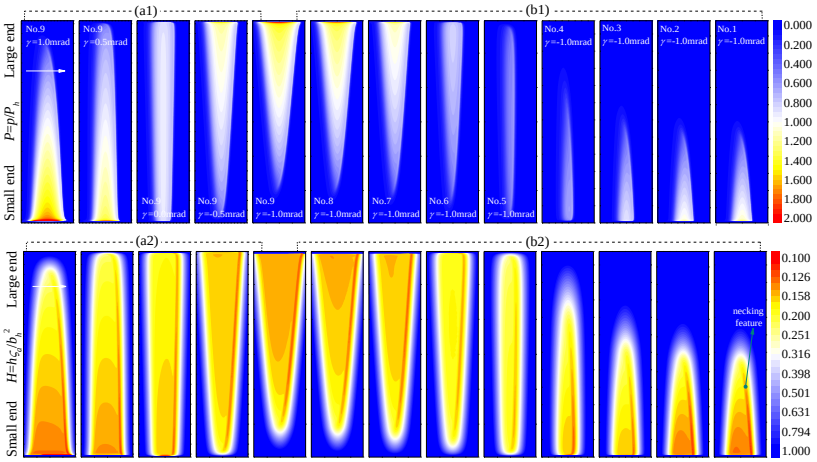

Figure 8. Film characteristics inside the TRB

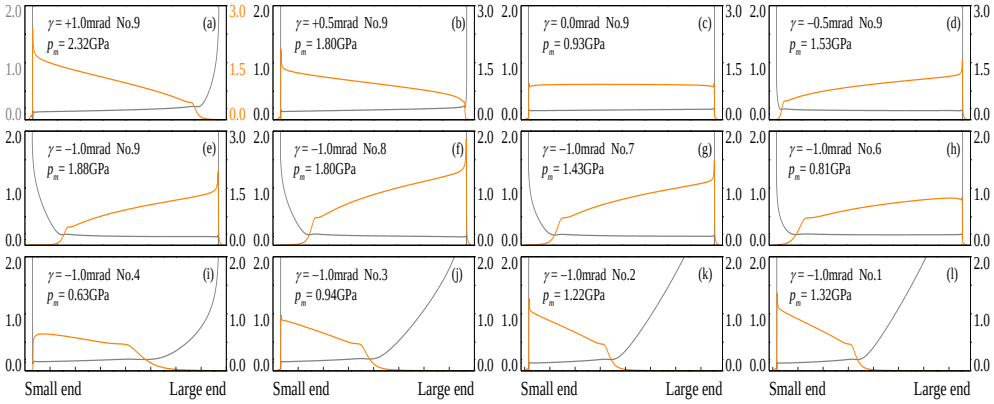

Figure 9. Grease film shape and pressure profile at y=0

3. 2. Constant Displacement Preload The constant displacement preload is a common preloading strategy for bearings. Figure 10(a, b) reveals the bearing condition of the TRB under the preload of δ_a=15μm and δ_a=30μm. In Figure 10(a), the load distribution varies with the shaft deflection is analogous to the constant force preload case, and the variation is more prominent. When the bearing with the radial load in Figure 10(b), it is substantially in a half-turn bearing state. If the shaft deflection continues to intensify, the half-turn bearing state would be changed.

In Figure 10(c, d), the variation and the amplitude of the roller tilt angle are basically consistent when the radial load F_z is 0 and -43kN. This is also reflected in Figures 3 and 7. Therefore, it can be inferred that the misaligned state of the roller is mainly produced by the external moment or shaft deflection, and is less affected by the radial load.

Using the results in Figure 10, the grease film at the TRB contacts was analyzed in three cases: 1) without the shaft deflection and with the radial load F_z, 2) with the shaft deflection and the load F_z, and 3) with the shaft deflection and without the load F_z. Figure 11(a) reveals the first case. The necking feature and pressure spike appear at the end of No. 9 roller, while the pressure profiles of other rollers are smooth. Note that the roller profile crowning can well ensure the film performance under this loading condition. The range of the pressure peak p_m is 0.01~0.85GPa. For No. 1 roller, the interaction of it with the cup is only 203.04N, but its deformation is obvious compared with the original profile.

Once the shaft is deflected, in Figure 11(b, c), the film characteristics are quite different from that without the shaft deflection, and their variations with the roller position are similar, whether or not the radial load F_z is applied. This is due to the fact that roller tilt is mainly affected by the deflected shaft. Meanwhile, significant film pressure spike and necking feature occur at roller-ends, especially for some light-loaded rollers, such as No. 1~3 rollers. The pressure peaks p_m at the contact edge

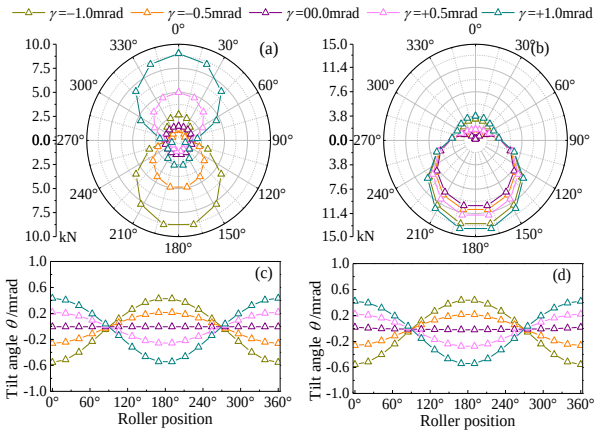

Figure 10. Bearing condition. (a, c) without radial load, F_z=0, δ_a=15μm. (b, d) with radial load, F_z=-43kN, δ_a=30μm

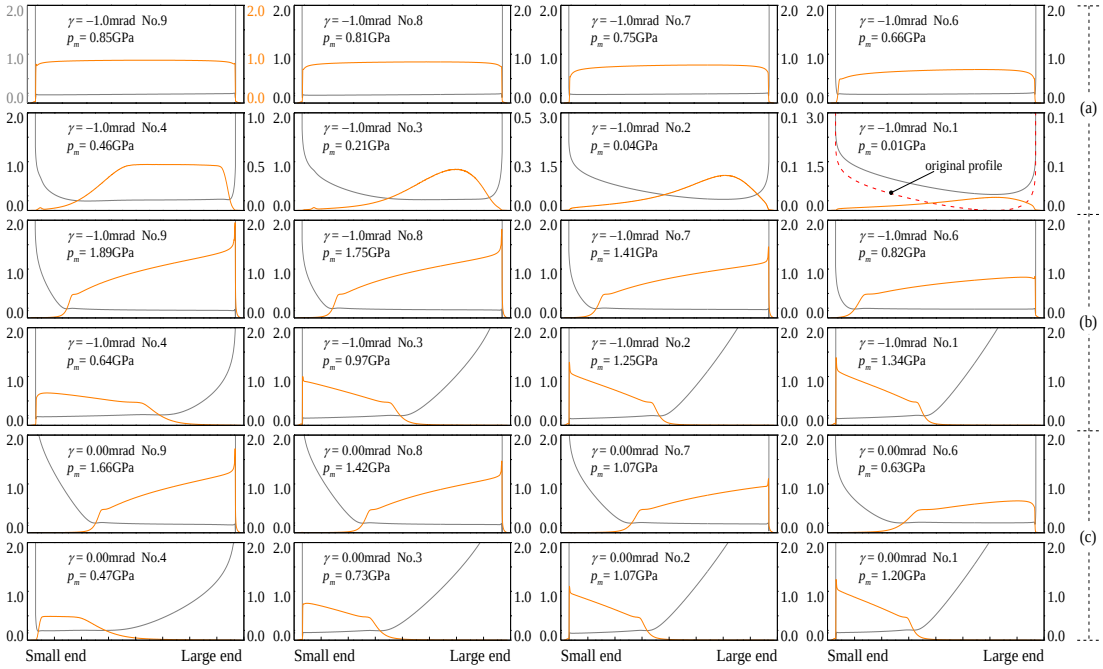

Figure 11. Grease film behavior under constant displacement preload. (a) F_z=-43kN, δ_a=30μm, γ=0mrad. (b) F_z=-43kN, δ_a=30μm, γ=-1mrad. (c) F_z=0, δ_a=15μm, γ=-1mrad

are in the ranges of 0.64~1.89GPa and 0.47~1.66GPa whether the force F_z is loaded or not. Since δ_a and F_z in Figure 11(b) are large, the roller contact length is generally longer than that in Figure 11(c), and the overall grease film is thinner. A common phenomenon is that the contact length of heavy-loaded rollers, as presented in Figure 6, 9 and 11(b, c), is greater than that of light-loaded rollers, even if they are in a severely tilted state. In summary, regardless of the TRB being preloaded by the force or displacement, the shaft misalignment has a negative impact on the bearing state and the film behavior at the bearing contacts.

4. CONCLUSION

The grease film characteristics inside the TRB subjected to the shaft deflection were addressed, negative effects of the misaligned shaft on bearing lubrication were clarified. The deflected shaft deteriorates the load-carrying capacity of the TRB. Roller tilt is mainly affected by the deflection and is less affected by the preload and radial load. When the shaft is in aligned state, rollers are all in a negative tilted state. The shaft deflection causes film characterizes at the TRB contacts to deviate from the normal state, and results in an irregular film shape and pressure profile. In addition, the deflection weakens the efficacy of the roller profile crowning, significant pressure spike and necking feature appear at the roller-end. Under loading conditions in this paper, the film thickness and pressure peak at the inner-race are thinner and greater than that at the outer-race, respectively. In the shaft-deflected state, the film thickness is reduced at some bearing contacts, but not much different in amplitude at all bearing contacts, and the film pressure peak has a large fluctuation.

The method in the paper is also applicable to the analysis of film behaviors inside oil-lubricated roller bearings in the shaft-deflected state. This study focused on grease-rich lubrication condition, the replenishment and starvation of the grease were neglected, which can be considered in the future work.

5. ACKNOWLEDGEMENT

The paper was supported by the National Natural Science Foundation of China (No. 51675427) and the Science and Technology Key Project of He'nan Province (No. 192102210026).

6. REFERENCES

1. Lugt, P. M., "A review on grease lubrication in rolling bearings", ***Tribology Transactions***, Vol. 52, No. 4, (2009), 470-480. doi: 10.1080/10402000802687940
2. Harris, T. A., "The effect of misalignment on the fatigue life of cylindrical roller bearings having crowned rolling members", ***Journal of Tribology***, Vol. 4, No. 2, (1969), 294-300. doi: 10.1115/1.3554918
3. Ebadi, P., Soleimani, M., and Beheshti, M., "Design methodology of base plates with column eccentricity in two directions under bidirectional moment", ***Civil Engineering Journal***, Vol. 4, No. 11, (2018), 2773-2786. doi: 10.28991/cej-03091197
4. Gurumoorthy, K. and Ghosh, A., "Failure investigation of a taper roller bearing: a case study", ***Case Studies in Engineering Failure Analysis***, Vol. 1, No. 2, (2013), 110-114. doi: 10.1016/j.csefa.2013.05.002
5. Dzyura, V. O., Maruschak, P. O., Zakiev, I. M., and Sorochaka, A. P., "Analysis of inner surface roughness parameters of load-carrying and support elements of mechanical systems", ***International Journal of Engineering, Transactions B: Applications***, doi. 30, No. 8, (2017), 1170-1175. Doi: 10.5829/ije.2017.30.08b.08
6. Zantopulos, H., "The effect of misalignment on the fatigue life of tapered roller bearings", ***Journal of Tribology***, Vol. 94, No. 2, (1972), 181-186. doi: 10.1115/1.3451678
7. Andréason, S., "Load distribution in a taper roller bearing arrangement considering misalignment", ***Tribology***, Vol. 6, No. 3, (1973), 84-92. doi: 10.1016/0041-2678(73)90241-8
8. Liu, J. Y., "Analysis of tapered roller bearings considering high speed and combined loading", ***Journal of Tribology***, Vol. 98, No. 4, (1976), 564-572. doi: 10.1115/1.3452933
9. De Mul, J. M., Vree, J. M., and Maas, D. A., "Equilibrium and associated load distribution in ball and roller bearings loaded in five degrees of freedom while neglecting friction-part II", ***Journal of Tribology***, Vol. 111, No. 1, (1989), 149-155. doi: 10.1115/1.3261865
10. Tong, V. C. and Hong, S. W., "Characteristics of tapered roller bearing subjected to combined radial and moment loads", ***International Journal of Precision Engineering and Manufacturing***, Vol. 1, No. 4, (2014), 323-328. doi: 10.1007/s40684-014-0040-1
11. Tong, V. C. and Hong, S. W., "The effect of angular misalignment on the running torques of tapered roller bearings", ***Tribology International***, Vol. 95, (2016), 76-85. doi: 10.1016/j.triboint.2015.11.005
12. Tong, V. C. and Hong, S. W., "The effect of angular misalignment on the stiffness characteristics of tapered roller bearings", ***Proceedings of the Institution of Mechanical Engineers, Part C: Journal of Mechanical Engineering Science***, Vol. 231, No. 4, (2017), 712-727. doi: 10.1177/0954406215621098
13. Kushwaha, M., Rahnejat, H., and Gohar, R., "Aligned and misaligned contacts of rollers to races in elastohydrodynamic finite line conjunctions", ***ARCHIVE Proceedings of the Institution of Mechanical Engineers, Part C: Journal of Mechanical Engineering Science 1989-1996***, Vol. 216, No. 11, (2002), 1051-1070. doi: 10.1243/095440602761609434
14. Panovko, M. Y., "Numerical modeling an elastohydrodynamic contact of shaped rollers with allowance for misalignment of their axes", ***Journal of Machinery Manufacture & Reliability***, Vol. 38, No. 5, (2009), 460-466. doi: 10.3103/S1052618809050094
15. Liu, X. L., Yang, P., and Yang, P. R., "Analysis of the lubricating mechanism for tilting rollers in rolling bearings", ***Proceedings of the Institution of Mechanical Engineers, Part J: Journal of Engineering Tribology***, Vol. 225, No. 11, (2011), 1059-1070. doi: 10.1177/1350650111413839
16. Liu, X. L., Li, S. Y., Yang, P., and Yang, P. R., "On the lubricating mechanism of roller skew in cylindrical roller bearings", ***Tribology Transactions***, Vol. 56, No. 6, (2013), 929-942. doi: 10.1080/10402004.2013.812760

17. Wu, Z., Xu, Y., and Liu, K., "The analysis on grease lubrication at two tapered bodies contact considering surface roughness", ***Forschung im Ingenieurwesen***, Vol. 83, No. 3, (2019), 339-350. doi: 10.1007/s10010-019-00350-9

18. Palmgren, A., "Ball and Roller Bearing Engineering", 3rd Edition, SKF Industries Inc., (1959).

19. Lundberg, G., "Elastische Berührung Zweier Halbräume", ***Forschung Auf Dem Gebiet Des Ingenieurwesens***, Vol. 10, No. 5, (1939), 201-211. doi: 10.1007/BF02584950

20. Shi, X. and Wang, L. Q., "TEHL analysis of aero-engine mainshaft roller bearing based on quasi-dynamics", ***Journal of Mechanical Engineering***, Vol. 52, No. 3, (2016), 86-92. doi: 10.3901/jme.2016.03.086

21. Huang, C., Wen, S., and Huang, P., "Multilevel solution of the elastohydrodynamic lubrication of concentrated contacts in spiroid gears", ***Journal of Tribology***, Vol. 115, No. 3, (1993), 481-486. doi: 10.1115/1.2921663.

22. Liu, S., Wang, Q., and Liu, G., "A versatile method of discrete convolution and FFT (DC-FFT) for contact analyses", ***Wear***, Vol. 243, No. 1-2, (2000), 101-111. doi: 10.1016/S0043-1648(00)00427-0

Persian Abstract

چکیده

خیز محور یکی از عوامل مهمی است که باعث تخریب حالت روان‌کاری گریس در یاتاقان‌های غلتکی مخروطی (TRB) می‌شود. بر این اساس، بنا بر فرضیه‌ی TRB، بارها و جابه‌جایی‌های خطی و پیچشی ایجاد شده در بخش‌هایی از یاتاقان تحت بارهای ترکیبی و پیچش محور در اثر بار حامل، تحلیل شد. سپس، ویژگی‌های لایه‌ی روان‌کار به منظور یافتن اثرات منفی خیز محور بر روی مشخصه‌های روان‌کار در کل یاتاقان بررسی شد. نتایج نشان داد که تاثیر خیز محور بر روی توزیع فشار در نبود بار شعاعی بیشتر از حالتی است که بار شعاعی بر غلتک وارد می‌شود. ناهم‌ترازی زاویه‌ای غلتک، معمولاً به دلیل خیز محور است. در نتیجه، خیز باعث نامنظم شدن شکل لایه‌ی روان‌کار و ایجاد پروفیل فشار در اتصالات TRB می‌گردد و فشار نقطه‌ای چشم‌گیر ایجاد می‌کند که منجر به بروز پدیده‌ی گلویی شدن در انتهای غلتک می‌شود.